Desalination and Water Treatment
www.deswater.com

doi: 10.5004/dwt.2020.26390

207 (2020) 30–42
December

Treatment by TiO_2/UV of wastewater generated in polymeric membranes production

Salomão de Andrade Pascoal[a], Camylla Barbosa Silva[a], Karyna Steffane da Silva[a], Geralda Gilvânia Cavalcante de Lima[a], Keila Machado de Medeiros[b], Carlos Antônio Pereira de Lima[a,*]

[a]*Sanitary and Environmental Engineering Department, State University of Paraiba, Av. Baraúnas, 351, 58429-500, Campina Grande, Paraiba, Brazil, Tel. +55 83 3315 3333; emails: caplima@uepb.edu.br (C.A.P. de Lima), salomaopascoal@hotmail.com (S. de Andrade Pascoal), camyllabsilva@hotmail.com (C.B. Silva), karynasteffane@hotmail.com (K.S. da Silva), gilvania@uepb.edu.br (G.G.C. de Lima)*
[b]*Science and Technology Center in Energy and Sustainability, Federal University of Recôncavo da Bahia, Av. Centenário, 697, Sim, 44042-280, Feira de Santana, Bahia, Brazil, Tel. +55 75 3622 9351; email: keilamedeiros@ufrb.edu.br*

Received 20 March 2020; Accepted 25 July 2020

ABSTRACT

Polyamide membranes play an important role in separation processes. However, the production of these membranes generates contaminated effluents with a high concentration of formic acid (FA), which is easily oxidized and highly toxic to the environment. Titanium dioxide (TiO_2) using ultraviolet (UV) radiation is a promising alternative for treating effluents contaminated by organic compounds. The objective of this article is to treat an effluent generated from the production of polymeric membranes, by the photocatalytic process. The TiO_2 particles were characterized by granulometric and textural analysis, scanning electron microscopy (SEM), thermal analysis, X-ray diffraction (XRD), and Fourier transform infrared (FTIR) spectroscopy. The effluent was characterized by the FA content and the chemical oxygen demand (COD). In the granulometric and textural analysis of TiO_2, it was found an average particle diameter of 59.6 nm and a specific surface area of 39.14 $m^2 g^{-1}$. By SEM, it was visualized that TiO_2 had a structure with particles of spherical format. Thermal analysis showed endothermic peaks up to 100°C, from water physically adsorbed on the surface of TiO_2. By XRD, it was observed that TiO_2 presented the crystalline phases anatase and rutile. Through FTIR, were found two bands of 505 and 612 cm^{-1} characteristic of TiO_2. In the physical–chemical analyzes 1,993.13 mg O_2 L^{-1} were obtained for COD and 106.45 mmol L^{-1} of FA content for the raw effluent. The treatment by UV radiation showed a low degradation of FA, while the technique with TiO_2/UV was more efficient, reaching 89.5% of degradation of FA and 79.44% in COD, presenting itself as a very promising process for the degradation of this effluent.

Keywords: Heterogeneous photocatalysis; Titanium dioxide; Ultraviolet radiation; Formic acid; Effluent treatment

1. Introduction

Water is undoubtedly a natural resource with economic value, as it is considered indispensable for the maintenance of all types of life on our planet. However, water scarcity is a current problem that affects various sectors of society, as it results from the precarious conditions of use or the lack of use of available water potentials, also compromising environmental sustainability.

Thus, it is necessary to search for technologies that provide quality water by viable methods, making this technology a target for the world market. With this, the

* Corresponding author.

development of membranes arises and plays an important role in the separation processes. Membrane filtration is a method widely used to separate small molecules such as salts, viruses, bacteria, or proteins in fluids. Currently, one of the most commonly applied methods for the production of porous membranes is based on the phase separation of polymer solutions [1]. Among the applications for water sanitation, polymeric membranes are very widespread in developed countries and are standing out in Brazil, as they are capable of separating substances that conventional filters cannot retain.

Membrane separation processes are generally considered to be green technology, with unique characteristics such as low energy consumption and compact and efficient operation. Although membranes have certainly improved the sustainability of chemical processes, it is not widely known that membrane fabrication itself is far from being a green process [2]. The manufacture of membranes by phase inversion, normally employs toxic dipolar aprotic solvents, such as formic acid (FA), *n*-methyl-2-pyrrolidone (NMP), and dimethylformamide (DMF) [3].

Polymeric membranes are produced by the phase inversion technique that can give rise to membranes with two layers, a selective (filtering skin) dense at the top and a porous layer at the bottom, with a significant variation in the size of pores along its thickness [4]. The phase inversion technique using the simple spreading immersion and precipitation method consists of immersing a flat polymeric film in a non-solvent bath. The transport of components is carried out between the two phases in contact, solvent for the bath and non-solvent for the film, causing the separation of the liquid–liquid phase and subsequent precipitation of the polymeric solution. This method allows great flexibility in the variation of the morphology, depending on which solvent and non-solvent is used [5,6]. Thus, this process generates a precipitation bath with a high percentage of solvent that must be reused in the same process or treated before disposal in the environment.

The process for obtaining these membranes by the immersion–precipitation method by phase inversion, produces a considerable volume of effluents that are inadequate to be discharged directly into the receiving water bodies. Therefore, studies on the treatment of these effluents, both for disposal and for the possibility of reusing treated water in the process itself are a growing necessity. The treatment of effluents generated in the membrane production processes is necessary, since it is highly harmful to the environment due, among other factors, to the high chemical oxygen demand (COD), and presence of various chemical compounds such as solvents and organic acids [7].

In the process of manufacturing polymeric membranes, the solvent *N*-methyl-2-pyrrolidone (NMP) is widely used in high concentrations such as 1,000 mg L^{-1}. Its disposal in the environment is very worrying, so treatment is necessary due to possible negative environmental impacts. Loh et al. [8] studied the treatment in a sequential batch reactor (SBR) as well as by a membrane bioreactor (MBR). The authors concluded that the treatment through the SBR was able to remove more than 90% of dissolved organic carbon and approximately 98% of the NMP in 2 h of experiment. However, the MBR experiment showed a decrease in efficiency from 100% to 40% in the period of 15 d of operation.

The use of DMF in the production of membranes is also very widespread, however due to its low degradability it demands an effective treatment of the generated effluents. Dou et al. [9] analyzed a new process for removing DMF in effluents. They used a process that combines extraction, distillation, and reverse osmosis (RO). In the distillation process, extractors were designed for the separation and recovery of the DMF, the simulations showed that more than 99% of the DMF could be recovered with 99% of purity.

Therefore, many processes have been proposed over the years and are currently being employed to destroy these pollutants. The so-called photocatalytic detoxification has been discussed as an alternative method for cleaning polluted waters [10]. In this regard, the advanced oxidative processes (AOPs) stand out, as excellent methods for the destruction of toxic pollutants in non-toxic substances. Among the AOPs, one can mention the heterogeneous photocatalytic process. Heterogeneous photocatalysis produces considerable amounts of hydroxyl radicals, which are a powerful oxidizing agent. Heterogeneous photocatalysis is becoming the future of water treatment, due to the addition of few chemicals, ease of implementation, and excellent cost-benefit of the industrial process [11].

Photocatalytic degradation is achieved with the aid of a photocatalyst, in this case a semiconductor, and a radiation source. It has as an advantage, the great efficiency in the degradation of toxic organic compounds without the need to resort to the use of other more energetic chemical oxidants, which, by themselves, are already highly pollutants [12]. The semiconductor is in a solid-state. The most used is titanium dioxide (TiO_2), which can be used for various applications because it is resistant to photo corrosion, has low cost, is non-toxic, and is photochemical and chemically stable over a wide range of pH [13].

Semiconductor photocatalysis involves activating the semiconductor by light. This light needs to have greater energy than that of the bandgap region, that is, the energy between the valence band (VB), where the electrons are attached to individual atoms and the conduction band (CB), where the electrons are free to move in the material's atomic network [14]. The oxidation capacity of photocatalysts can be regulated through semiconductor band-gap engineering, which has an extremely high selectivity for the target product to be achieved [15].

TiO_2 absorbs light energy ($\lambda\nu$) in the ultraviolet range (<254 nm) from natural (sun) or artificial sources (lamps). As shown by the equations below, the light energy absorbed by the semiconductor results in the generation of electron pairs/gaps ($e^- + h^+$) [Eq. (1)] that will produce reactive radicals, hydroxyls ($OH^\bullet$) [Eq. (2)], which will oxidize and mineralize organic compounds [Eq. (3)] [16,17]:

$$TiO_2 + \lambda\nu \rightarrow TiO_2\left(e^- + h^+\right) \quad (1)$$

$$H_2O + TiO_2\left(h^+\right) \rightarrow TiO_2 + OH^\bullet + H^+ \quad (2)$$

$$OH^\bullet + \text{Organic compounds} \rightarrow H_2O + CO_2 \quad (3)$$

The organic pollutants adsorbed on the catalyst are then degraded by successive radical reactions in non-toxic products and mineral species. The degradation capacity of the semiconductor is related to several parameters, such as the nature and intensity of radiation from the light source, the number of incident photons for the activation of TiO_2, the nature of the reaction medium, the amount of TiO_2 (or active sites), the water content for the production of hydroxyl radicals and the nature and concentrations of pollutants [18].

Therefore, when exposed to water containing a high concentration of FA obtained by the production process of polymeric membranes by the phase inversion technique, it significantly changes the quantity and size of the pores on the surface and cross-section of these membranes. Thus, to reuse this water, it is interesting that it contains up to 30% FA in the precipitation bath, so that the membranes obtained have adequate morphology and microstructure to be used in microfiltration processes in the treatment of liquid effluents [19,20].

Sadi et al. [21] evaluated the treatment of FA through the photocatalytic activity of TiO_2. The addition of quaternary ammonium bromide as a co-catalyst was investigated in order to assist growth at low temperatures in the anatase phase. The photodegradation of FA was selected as a reaction model because it undergoes direct mineralization to CO_2 and H_2O without the formation of stable intermediate species. In addition, this compound represents a possible final step in the photodegradation of more complex organic compounds. A complete kinetic study for photodegradation of FA was performed to better understand the results. The modified TiO_2 was investigated in the photodegradation of FA under ultraviolet light, revealing interesting photocatalytic properties. The maximum photocatalytic activity was reached for a content corresponding to a maximum recovery by monolayer of FA on the surface of TiO_2.

The objective of this work is to evaluate the photocatalytic degradation of effluents generated by the production of polymeric membranes, analyzing the degree of reduction in FA and removal of COD. The initial concentration of the effluent and the effect of the photocatalyst load were examined.

2. Experimental

2.1. Chemical products

The photocatalyst used in this study for the treatment of the effluent was titanium dioxide (TiO_2) which is presented as a fine powder (a mixture of two phases, 80% anatase and 20% rutile) supplied by Degussa®, with a molecular structure shown in Fig. 1a. The effluent used came from the Membrane Development Laboratory of the Federal University of Campina Grande, Paraiba, Brazil. The polymeric and hybrid membranes were obtained using the phase inversion technique, formed by the polymer, inorganic fillers, and the solvent, resulting in the formation of the effluent. Its major compound is the organic solvent FA with a molecular formula CH_2O_2, which has a molar mass of 46.03 g mol^{-1}, with molecular structure shown in Fig. 1b.

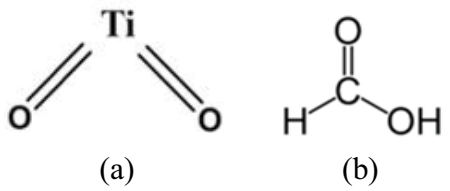

Fig. 1. Molecular structure (a) TiO_2 and (b) FA.

2.2. Characterization of titanium dioxide

The granulometric distribution was performed in a Mastersizer 2000 of Malvern, Instruments Ltd., (Malvern, United Kingdom). In this method, the proportional relation between laser diffraction, concentration and particle size is combined. The equipment used to obtain the specific surface area, the pore volume and the average pore diameter was a textural analyzer Quantachrome Nova 3200e model (USA). Analysis of scanning electron microscopy (SEM) was performed on the Tescan Analytics Equipments (Brno, Czech Republic), model Vega 3, operating at 20 kV. A morphological analysis of the surface of TiO_2 was performed. The material was sprayed with gold on the Shimadzu IC sputter 50 equipment (Tokyo, Japan), using a current of 4 mA for a period of 3 min. The mass loss was obtained by thermogravimetry (TG) in a thermobalance model Shimadzu TGA-60 (Tokyo, Japan) in nitrogen atmosphere with alumina crucible, flow of 50 mL min^{-1} and heating rate 10°C min^{-1}, from room temperature to 1,000°C. Differential scanning calorimetry (DSC) was performed on DSC-50 equipment from Shimadzu (Tokyo, Japan), with scans that started at room temperature up to 350°C, at a heating rate of 10°C min^{-1}, under nitrogen atmosphere. X-ray diffraction (XRD) analysis for TiO_2 was conducted on a Shimadzu XRD-6000 diffractometer instrument (Tokyo, Japan), using copper Kα radiation (λ = 1.541 Å), 40 kV of voltage, current 30 mA, scanning from 2 to 75 with a scan rate of 2 min^{-1}. The analysis of Fourier transform infrared spectroscopy (FTIR) was performed on a PerkinElmer Analytical Instruments (Massachusetts, United States) Spectrum 400 spectrometer with scan from 4,000 to 400 cm^{-1}. All analyses were performed in the Materials Characterization Laboratory of the Academic Unit of Materials Engineering at the Federal University of Campina Grande.

2.3. Effluent characterization

The phase inversion technique is the most common method for the production of polymeric membranes based on the separation of an initially homogeneous system into two distinct phases consisting of the polymeric membrane and an effluent with a high concentration of FA and possibly other additives in small amounts, such as inorganic salts that act as porogenic agents forming the membrane pores. The effluent was characterized by the COD and the FA content as it is the major compound in obtaining the membrane, the methodology for determining FA and COD were, organic and volatic acids/distilation method (5,560 D) and closed reflux titrimetric method (5,520°C), respectively, described in Baird et al. [22]. COD is an extremely important measurement in the treatment of effluents, as it

is an indirect measurement of the amount of organic matter present in it, with this determination, it is possible to measure virtually all organic compounds that can be leftover from the photocatalytic treatment. The analyzes for the characterization of the effluent were carried out at the Environmental Sciences Research Laboratory of the Department of Sanitary and Environmental Engineering at the State University of Paraiba.

2.4. Experimental planning

In order to improve the process of heterogeneous photocatalysis in the treatment of effluents generated in the production of polymeric membranes, an experimental planning was carried out with two factors and two levels 2^2 with two central points for the TiO_2 content, in which six experiments were obtained to be performed. It was defined the TiO_2 load low, (0.1), medium (0.3), and high (0.5)% m/m, initial concentration of FA to be low (1.2) and high (2.4) mmol L^{-1}.

The experimental planning consists of analyzing the effluent degradation in view of the influence of the parameters: load of the photocatalyst and initial concentration of the FA. Table 1 show the experimental matrix used in this research.

2.5. Photolytic and photocatalytic process

The experiments were carried out in two stages: first, with UV radiation and absence of catalysts (photolysis), and a second, with UV radiation and the presence of the photocatalyst (TiO_2). The photocatalytic experiments were conducted in the presence of the photocatalyst, with varying amounts of (TiO_2), which were 0.1%, 0.3%, and 0.5%.

The experimental system consists of a wooden box (Fig. 2), with a glass door on its front, for viewing its interior. On the top of the box there are three 15 W germicidal lamps (Philips) that emitted ultraviolet radiation (UV) at a wavelength of 254 nm. Inside the box there is a cylindrical shaped reactor made of Pyrex glass with a volume of 1,000 mL. All experiments were carried out at a temperature of approximately 23°C (room temperature).

In the photocatalysis, suspensions with the presence of TiO_2 were stirred in the dark for 30 min to achieve the adsorption/desorption equilibrium of the FA present in the effluent. The adsorption equilibrium studies were performed in the period of contact of TiO_2 with the effluent in the absence of light. The volume of effluent used in each experiment was 1,000 mL, the effluent remained in the reactor for 4 h and was kept in suspension under constant agitation with the use of an electromagnetic stirrer, being exposed to UV radiation. During this period, every 30 min, a 30 mL sample was taken to monitor the degradation process. The samples that contained the photocatalyst were centrifuged with a rotation speed of 4,000 rpm, in a centrifugal equipment manufactured in Brazil, type Fanem Excelsa II 206BL, for 30 min so that the sedimentation of the suspended photocatalyst could occur. With the supernatant material, the physical–chemical characterization of the samples was carried out to monitor the COD variation rate and the FA concentration. The experiments were carried out at the Environmental Sciences Research Laboratory of the Department of Sanitary and Environmental Engineering of the State University of Paraiba.

3. Results and discussion

3.1. Characterization of TiO_2

The characterization of commercial TiO_2 (Degussa P25) was carried out, to prove that its physical–chemical properties, intrinsic characteristics, and efficiency were preserved and suitable for application in heterogeneous photocatalysis. The characteristics include nanometer-scale particles, high specific surface area, volume and average pore diameter (mesoporosity), spherical shape morphology, crystalline phases and planes mostly anatase, wavelength with vibration of Ti–O bonds, and their thermal properties, confirming the transitions of the amorphous phase of the material.

3.1.1. Granulometric and textural analysis

Fig. 3 illustrates the particle size distribution and the average diameter of the TiO_2 particles.

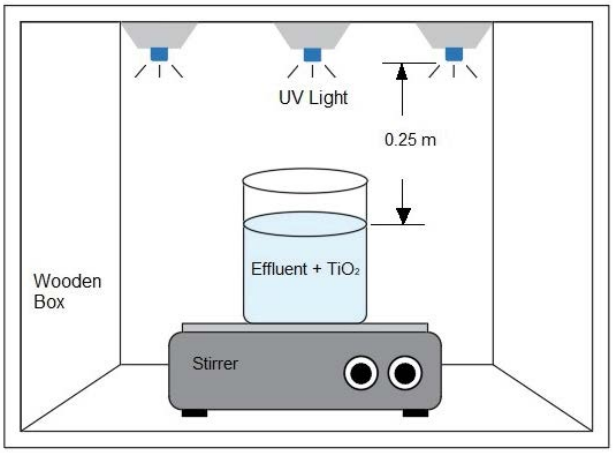

Fig. 2. Photocatalytic reactor.

Table 1
Experimental matrix

Parameter	Treatment					
	*T*1	*T*2	*T*3	*T*4	*T*5	*T*6
TiO_2 (%) load	0.1	0.1	0.3	0.3	0.5	0.5
Initial FA concentration (mmol L^{-1})	1.1	2.2	1.2	2.4	1.2	2.4

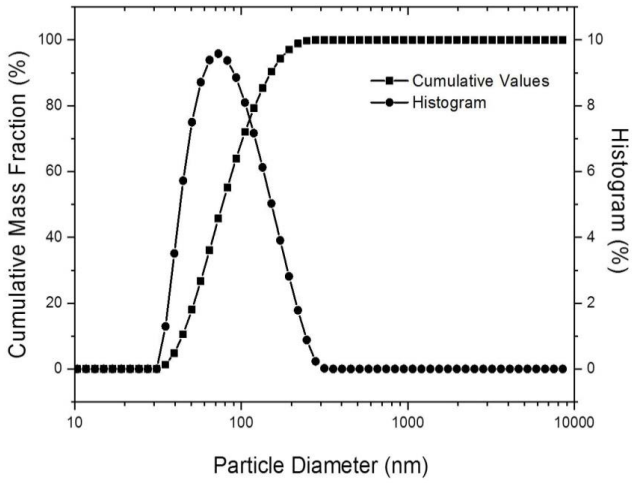

Fig. 3. TiO_2 granulometric distribution.

Knowledge of the statistical granulometric distribution and the size of elementary particles is essential, as it significantly influences the microstructure, affecting the density, thermal, electrical, and photocatalytic properties of the semiconductor. Therefore, determining the particle size of TiO_2 and proving its nanoparticles by means of particle size distribution is extremely important to act more efficiently in the photocatalytic process. In Fig. 3, it can be seen that the frequency histogram curve for the TiO_2 particle size distribution is unimodal with a distribution range with an average particle diameter of 59.6 nm. The size distribution range extends from 30 to 300 nm [23,24]. About 57.35% by mass of the accumulated particles are smaller than 87.8 nm. The narrower the distribution shown by the particle diameter curve, the greater the homogeneity in relation to the particle distribution, size, and geometry.

Also according to Fig. 3, the d_{10} = 10% of the particles obtained was with diameters less than 46.1 nm, d_{50} = 50% of the particles had diameters less than 76.8 nm and d_{90} = 90% of the particles was with diameters less than 158.6 nm [25]. Furthermore, the decrease in particle size is accompanied by an increase in the surface/volume ratio, which makes the surface energy contribute significantly to the total energy of the material. This means that, for small particles, the polymorphic form with the lowest surface energy exhibits the highest thermodynamic stability, which contributes to a better performance of the photocatalytic process [26].

Table 2 illustrates the values of the textural analysis that correspond to the specific surface area (S_{BET}) that was determined by the Brunauer–Emmett–Teller (BET) method developed by Stephen Brunauer, Paul Hugh Emmett, and Edward Teller, and the pore volume (V_p) and average pore diameter (D_p) that were calculated by the Barrett–Joyner–Halenda (BJH) method that was described by Barrett–Joyner–Halenda.

The BET method describes the physical adsorption of gas molecules on a solid surface and serves as a basis for an important analysis technique for measuring a specific surface area of a material. The S_{BET} obtained in Table 2 was 39.14 $m^2\ g^{-1}$, which is considered a high value of surface area that is favorable to improve the catalytic activity, the same resulting from small particles or porous structure [27,28]. The photocatalytic activity of TiO_2 depends on a large number of parameters, including the crystalline structure, the relationship between the anatase and rutile phases, the particle size, the specific surface area, and the average pore size [29].

Table 2
TiO_2 textural analysis

Textural analysis	TiO_2
Specific surface area ($m^2\ g^{-1}$)	39.14
Pore volume ($cm^3\ g^{-1}$)	0.034
Average pore diameter (nm)	2.26

The adsorption of nitrogen using the BJH method provides information on the mesoporosity of the material. According to the result obtained from V_p = 0.034 $cm^3\ g^{-1}$, in addition to a D_p = 2.26 nm (Table 2) that can be classified as a material with mesoporous structure (pore width in the range of 2–50 nm) according to the International Union of Pure and Applied Chemistry (IUPAC) classification, with pores being filled by: pore condensation, which reflects a first-order gas–liquid phase transition [30]. The IUPAC classification is based on measurements of adsorption and desorption of nitrogen gas at its boiling temperature, and on the statistical width of the adsorbed N_2 gas layers. Mesoporous TiO_2 is the result of pores formed in its particles, presenting a large surface area due to a porous confined structure and a high surface/volume ratio [31]. Furthermore, mesoporosity is related to the presence of cavities, channels, or interstices, which are capable of interacting with atoms, ions, molecules, and nanoparticles, not only on their surfaces, but also throughout the mass, making it of great importance in photocatalytic applications.

3.1.2. Scanning electron microscopy

SEM photomicrographs were necessary to study the microstructure of TiO_2, identifying the size, shape, and quantity of particle agglomerates, as shown in Fig. 4.

From the photomicrographs, it can be seen in Figs. 4a–e, with magnifications of 500×; 1,000×; 2,000×; 3,000×; and 5,000×, respectively, that the samples have a morphological variation over their surface area, with the presence of large clusters of particles with different sizes, without defined shapes, with little homogeneous distribution of these aggregates. Most commercially available nanoparticles are large clusters of about 1 μm in maximum size, composed of primary particles with sizes ranging from 5 to 50 nm. Large clusters disperse light and are not directly suitable for optical systems [32]. The primary particles can be held together by weak Van der Waals interactions in the case of clusters or by strong interactions in the case of aggregates. The degree of agglomeration of the TiO_2 particles depends on factors such as the pH of the suspension, the ionic strength, the size of the particles, and the concentration of particles [33].

In Figs. 4f–i, with increases greater than 8,000×; 10,000×; 15,000×; and 20,000×, respectively, morphological structures with particles on the micrometric scale were observed,

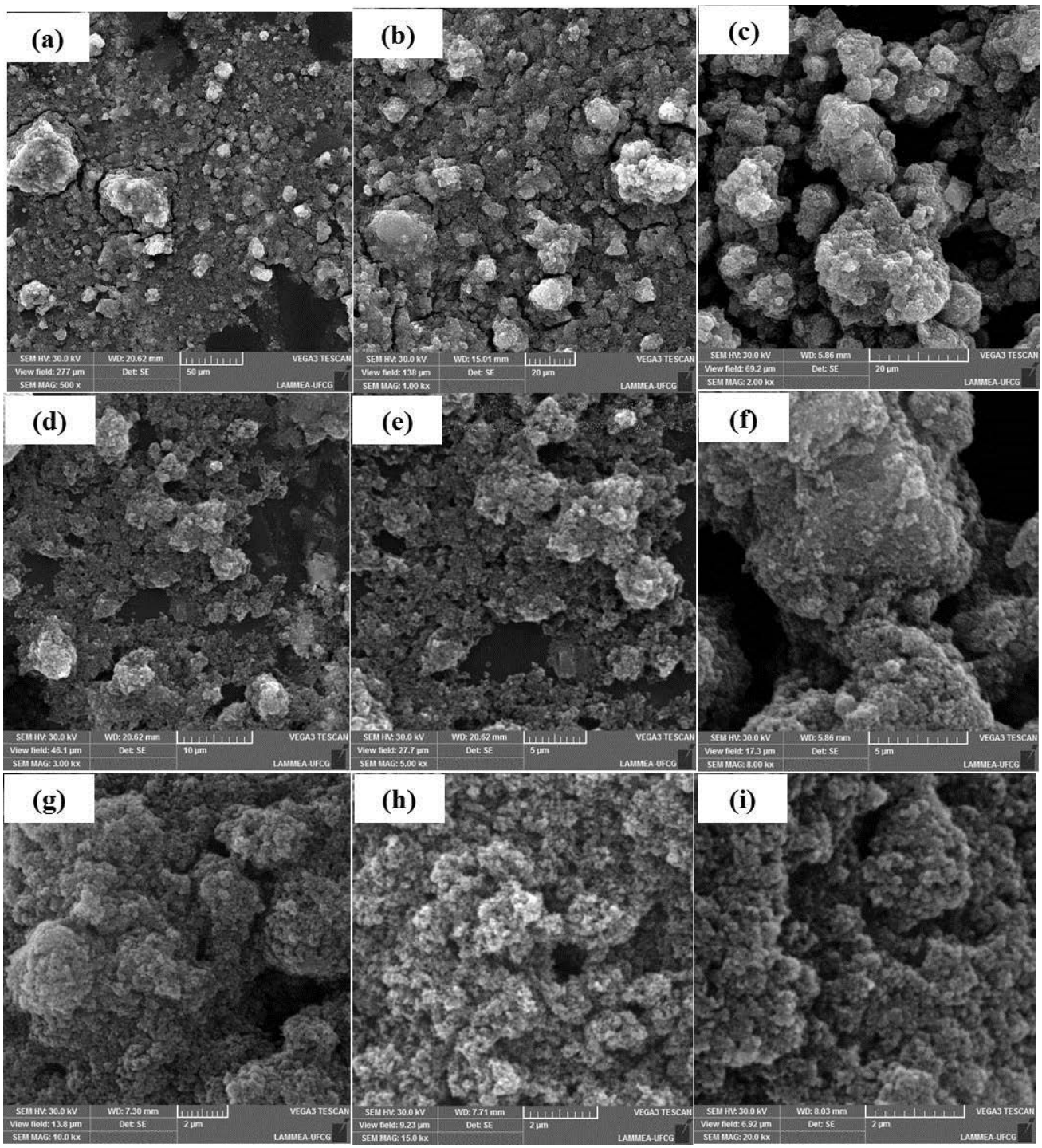

Fig. 4. SEM photomicrograph of titanium dioxide with magnifications of: (a) 500×, (b) 1,000×, (c) 2,000×, (d) 3,000×, (e) 5,000×, (f) 8,000×, (g) 10,000×, (h) 15,000×, and (i) 20,000×.

with spherical shapes and uniformly distributed [34]. In addition, from these increases, a microporous structure became more evident on its surface and between the TiO_2 particles. Therefore, the microstructure of TiO_2 particles obtained, favored its application in the photocatalytic process, because many factors have a significant influence on performance, including size, specific surface area, pore-volume, pore structure, crystal phase, and the aspects that the semiconductor surface is exposed [35].

3.1.3. Thermal analysis

Thermal analysis is the study of the relationship between a sample property and its temperature as the sample is

heated in a controlled manner, as an example, we have DSC and thermogravimetry/differential thermogravimetry (TG/DTG). These techniques are used to provide qualitative, semi-quantitative, and even quantitative measurements of energy evolution in heating materials over a considerable temperature range. Figs. 5 and 6 illustrate the DSC and TG/DTG curves of TiO_2, respectively.

DSC is a technique used to determine the heat flow inside and outside a sample when subjected to a controlled atmosphere temperature program. In the DSC curve, when heating a sample, thermal changes in a material are accompanied by a heat exchange; hence the temperature of these transformations and heat flow can be determined. In Fig. 5, two endothermic events can be observed: at 54°C, which may be related to the physiosorption of water on the surface; and at 218°C it can be attributed to the water leaving the constitution and formation of TiO_2 [36]. It is important to note that a wider temperature range up to 1,000°C could reveal other events, which would make it possible to attribute the transition temperatures from amorphous phase to anatase and from anatase to rutile. However, the DSC analysis instrument used did not allow to obtain events above 350°C, so it was necessary to perform a TG to increase this temperature range and to be able to observe the phase transitions that occurred in TiO_2.

TG follows mass changes in a sample subjected to heat treatment. A TG can be recorded as a change in the sample's mass with temperature and time, and with the pressure and gas composition. From the TG curve and its derivative illustrated in Fig. 6, a total mass loss of 4% for TiO_2 was evidenced and the mass loss events detected occurred in four stages of decomposition: at 4°C referring to water desorption; at 262°C inherent in the loss of crystalline TiO_2 water, eliminating hydroxyl group as water vapor by condensation of Ti–OH groups, producing the Ti–O–Ti bond; at 483°C related to the conversion of $Ti(OH)_4$ to TiO_2, indicating the beginning of the structural organization of the system, which possibly will induce the crystallization of the amorphous phase for anatase; and at 623°C it probably corresponds to the transition from the anatase phase to rutile phase [37–39].

According to DSC and TG/DTG of Figs. 5 and 6, it was found that the endothermic peaks between room temperature up to 100°C came from free water and from water molecules physically adsorbed on the TiO_2 surface by hydrogen bonds, since both water molecular as the dissociated (–OH groups) adsorbed on semiconductor, end up favoring the photocatalytic process [40,41].

3.1.4. X-ray diffraction

By XRD, it was possible to identify the phases and crystalline planes of the sample, as can be seen in Fig. 7.

According to the diffractogram shown in Fig. 7, it can be seen that the crystalline phases characteristic of TiO_2 were anatase and rutile. The diffraction peaks characteristic of the anatase phase of TiO_2 are 2θ = 25.4°, 37.9°, 38.4°, 38.7°, 48.3°, 54.0°, 62.2°, 62.9°, 68.8°, 70.5°, and the crystalline planes (101), (103), (004), (112), (200), (105), (213), (204), (116), and (220), respectively. Also in the XRD standard, peaks characteristic of the rutile phase TiO_2 were visualized at 2θ = 37.8°, 44.5°, 55.5°, and 64.8° and crystalline planes

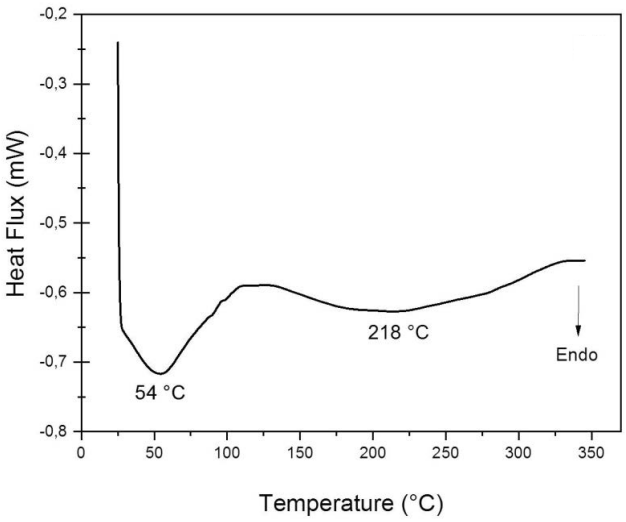

Fig. 5. TiO_2 DSC curves.

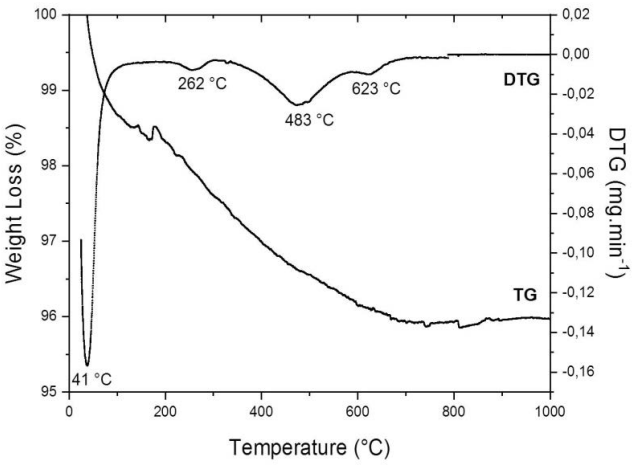

Fig. 6. TiO_2 TG/DTG curves.

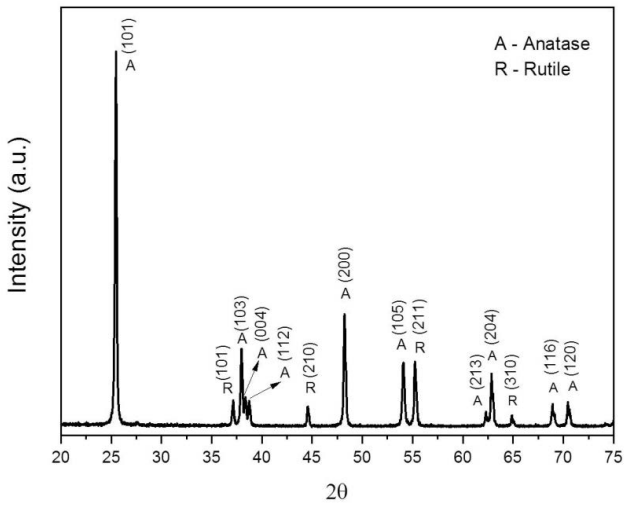

Fig. 7. TiO_2 XRD diffractogram.

(101), (210), (211), and (310), respectively [42,43]. Therefore, the samples prevailed in the anatase phase, confirming that the material used as a source of TiO_2 was Degussa P25, which consists of 70% anatase and 30% rutile [44]. The photocatalytic activity of TiO_2 is strongly dependent on the size of its crystallite, the relationship between the anatase and rutile phases and phase structure, the particle size, specific surface area, and the average pore size. Due to a greater gap (3.2 eV) of anatase than rutile (3.0 eV), anatase has less sunlight absorption capacity than rutile [45]. This is due to the rate of recombination of carriers of lower anatase load and greater surface adsorption capacity to hydroxyl groups than rutile [46]. Crystalline anatase is the largest phase, this characteristic is important because it is the most photoactive phase of titanium dioxide, which is highly desirable in processes of photocatalytic degradation [47,48].

3.1.5. Fourier transform infrared spectroscopy

The results of the FTIR analysis of the characteristic bands of titanium dioxide can be seen in Fig. 8. It was observed by the band of the FTIR spectrum, the band 505 cm^{-1} which is due to the vibration of the Ti–O connection [49] and the band at 612 cm^{-1} which is attributed to the vibration of the Ti–OO connection [50]. A peak observed in the range between 403 and 978 cm^{-1} was due to the vibrations of six coordinated TiO_6 octahedrons and four by coordinated titanium anatase of Ti–O titration. The band at 1,638 cm^{-1} is assigned to the vibration mode of the H–O–H connection of the physisorbed water [51]. The 2,378 cm^{-1} range is attributed to the CO_2 present in the atmosphere [52]. For the TiO_2 sample, the spectrum shows a strong absorption band at 3,426 cm^{-1}, corresponding to the isolated –OH, related to the stretching frequency of –OH attributed to the surface of water adsorbed by the TiO_2 sample. The amount of O–H groups adsorbed on the catalyst surface is responsible for improving the photocatalytic efficiency [53].

3.2. Effluent characterization

Initially, the characterization of the effluent from the membrane production process was carried out, and physical–chemical analyzes were executed, in which the COD values of 1,993.13 mg O_2 L^{-1}, and FA content with 106.45 mmol FA L^{-1} and pH 2.4 were determined. Szekely et al. [54] show that after manufacturing membranes by phase inversion process, solvents and toxic additives such as plasticizers in the casting solution (generally between 75 and 85 weight%) remain in the non-solvent bath, generating a large amount of liquid waste. This proved the great polluting potential of this type of effluent. Then, initial tests of degradation of the raw effluent were carried out and it was found that with a high concentration of FA, its degradation is not satisfactory. Because to degrade organic compounds with a high polluting load it is necessary to increase the photocatalyst content, however a greater amount of TiO_2 prevents the proper penetration of UV radiation, making the process inefficient. Therefore, dilutions of the raw effluent were made with distilled water to preserve its characteristics, to the concentrations of 1.2 mmol FA L^{-1} (pH 3.4) and 2.4 mmol FA L^{-1} (pH 3.2) for the FA content, then COD determinations for these concentrations were performed, obtaining 164.44 and 204.59 mg O_2 L^{-1}, respectively. Riboni et al. [55] studied the degradation of FA, with a mixture of TiO_2 and Ti-W oxide photocatalysts, using a low acid concentration, obtaining a 95% degradation of the acid. The acid concentration used for this degradation was 1.0 mmol L^{-1}. Ardila et al. [56] studied the degradation of FA (0.22 mmol L^{-1}) and phenol (0.1 mmol L^{-1}) using commercial titanium dioxide in a UVA-LED photocatalytic reactor in batch mode with recirculation, where they obtained about 72% and 60% of the removal of COD and TOC, respectively, after 60 min of irradiation with TiO_2, carrying 0.5 g L^{-1}.

3.3. Photolytic and photocatalytic processes

Direct photolysis is the transformation of a compound as a result of its own light absorption. Heterogeneous photocatalysis designates the activation of a semiconductor by means of natural or artificial light. A semiconductor like TiO_2 is used as a photocatalyst because they have an electronic configuration characterized by having a valence band (VB) that is filled with electrons and a conduction band that is an empty conduction band (CB). Thus, the difference between these two bands is a small and well-defined energy value known as a bandgap, which means an interval between the bands [57].

Fig. 9 shows the effect of the irradiation time for the photocatalytic degradation process, for two initial concentrations of the FA and three loads of the photocatalyst, and for the process of photolysis of the effluent with the monitoring of the concentration of the FA. According to the data obtained, it was possible to observe that the photolysis was not efficient for the degradation of the FA, reaching a low removal. The concentration of 1.2 mmol FA L^{-1} showed a removal of 6.10% and the concentration of 2.4 mmol FA L^{-1} removed 13.92% [58]. The degradation of the effluent with the presence of irradiation alone, under the same conditions for the photocatalytic process, can be detected as a standard measure of the photocatalytic activity for an effluent with organic pollutants.

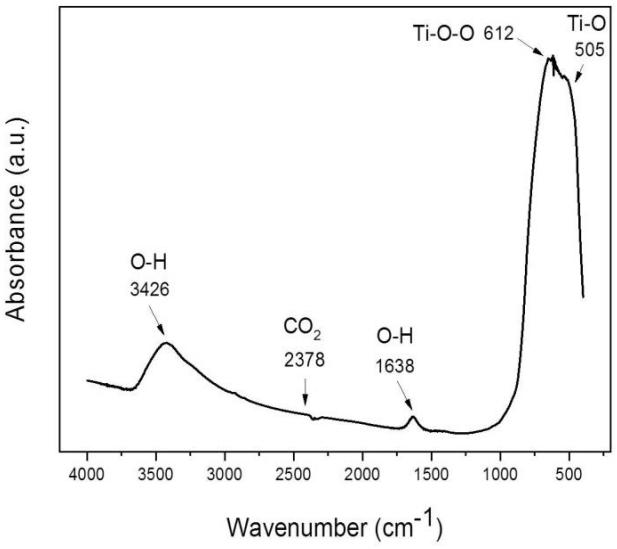

Fig. 8. TiO_2 FTIR spectrum.

Also, in Fig. 9, it is shown the photocatalytic process of the degradation of the FA. In the first 30 min in which the effluent was in the dark (without the presence of radiation), it was possible to notice that there is no type of degradation, for the two levels of initial effluent concentrations. With the increase in the exposure time of the effluent to radiation, the degradation happened gradually. However, the difference in degradation that exists between the different loads of the photocatalyst is negligible, as they present an extremely low difference in degradation when compared to one another. It is still possible to observe that degradation of the FA after 240 min does not occur entirely, this fact may probably have occurred due to inorganic compounds present in the composition of the hybrid membranes obtained by the phase inversion technique. This influence was also observed by Negishi et al. [59], who studied the degradation of FA by photocatalysis with TiO_2/UV, noted that the rate of degradation of FA decreased with the increase of inorganic substances present in the effluent. Using titanium dioxide together with graphene particles, GA-TiO_2 (anatase/rutile-87/13%), Hamandi et al. [60] degraded FA at a concentration of 21.7 mmol L^{-1}, reaching 60% efficiency. Therefore, we have to carry out experiments with an initial concentration of 1.2 mmol FA L^{-1}, which showed 72.61% FA removal for 0.1% TiO_2 load, 76.52% for 0.3% load, and 80.44% for 0.5% load. For the initial concentration of the 2.4 mmol FA L^{-1} effluent, it was found that for the 0.1% load of TiO_2, 80.44% was degraded, for the 0.3% load, it was degraded 84.35%, and for the 0.5% load, 88.26% was degraded.

Therefore, it is important to highlight that for the degradation of the FA, the best parameters relating to the initial concentration of the effluent and the load of the photocatalyst were observed with the initial concentration of 2.4 mmol FA L^{-1} and the charge of the photocatalyst of 0.5%, with an acid removal of 88.26%.

3.4. Degradation mechanism

The degradation mechanism of FA was studied by El-Alami et al. [61] in which they proved that this degradation can occur through the reaction of adsorbed FA (ads) or FA present in the solution/surface interface of the catalysts (inter) with the surface of the hydroxyl radicals ($OH^{\bullet}_{surf}$) or holes [reactions (4) and (5), respectively] or through the reaction of FA in aqueous solution with free hydroxyl radicals ($OH^{\bullet}_{free}$) [reaction (6)].

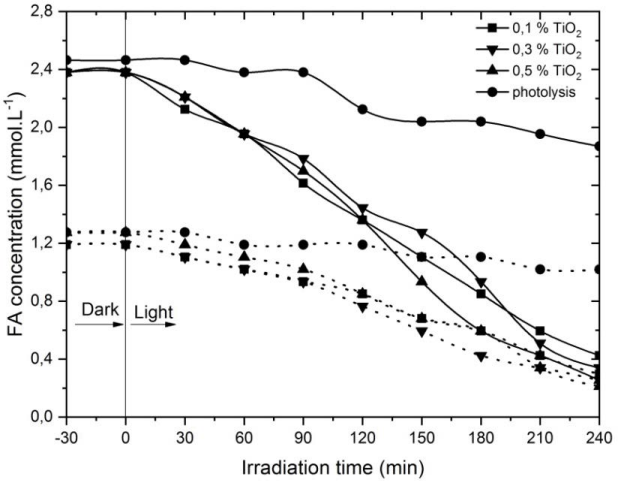

Fig. 9. Efficiency of photolytic and photocatalytic processes (- - -) 1.1 mmol FA L^{-1}; (—) 2.2 mmol FA L^{-1}.

$$HCOO^-_{(ads)/inter} + OH^{\bullet}_{surf} \rightarrow CO_2^{\bullet -} + H_2O \quad (4)$$

$$HCOO^-_{(ads)/inter} + H^+ \rightarrow CO_2^{\bullet -} + H^+ \quad (5)$$

$$HCOO^-_{(aqu)} + OH^{\bullet}_{free} \rightarrow CO_2^- + H_2O \quad (6)$$

According to Miller et al. [62] who studied the effect of water on the photocatalytic decomposition of FA in TiO_2 and Pt/TiO_2, it was verified that this decomposition of FA forms CO_2 and H_2O with TiO_2, but forms CO_2 and H_2 with Pt/TiO_2. Thus, during the photocatalytic decomposition of FA with TiO_2, the FA extracts a cross-linked oxygen from TiO_2 to produce CO_2 and H_2O at room temperature, this creates an oxygen vacancy which decreases the rate of decomposition.

3.5. Kinetic analysis of photocatalytic degradation

The photocatalytic degradation of the FA obeys the pseudo-first-order of kinetics in terms of the modified Langmuir–Hinshelwood (L–H) model by Eq. (7):

$$r = -\frac{dC}{dt} = \frac{k_r \cdot k_a \cdot C}{1 + k_a \cdot C} \quad (7)$$

In this Eq. (7), r (mmol L^{-1} min^{-1}), k_r (mmol L^{-1} min^{-1}), k_a (L $mmol^{-1}$), C (L $mmol^{-1}$), and t (min) are the reaction rate, reaction rate constant, adsorption constant, reagent concentration, and irradiation time, respectively [63–66]. At the low initial dye concentration, the rate expression [Eq. (7)] can be written in the form of Eq. (8):

$$r = -\frac{dC}{dt} = k_r \cdot k_a \cdot C = K \cdot C \quad (8)$$

where K is the pseudo-first-order rate constant and by integrating Eq. (7) with the limit of $C = C_0$ at $t = 0$, it changes to Eq. (9):

$$\ln\left(\frac{C}{C_0}\right) = -k \cdot t \quad (9)$$

In Eq. (9), C_0 is the initial concentration and C is the sum of the surface and solution concentrations of the dye at each moment. According to Eq. (9), the graph of $\ln(C/C_0)$ vs. t for all concentrations must be linear and the values of k can be obtained directly through its slope. One of the most useful indications for assessing the reaction rate of first-order-kinetics is the calculation of the half-life reaction. The half-life ($t_{1/2}$) was calculated by Eq. (10) as follows:

$$t_{1/2} = \frac{\ln(2)}{k} \quad (10)$$

Figs. 10 and 11 show the $\ln(C/C_0)$ as a function of time and represent a straight line. The slope of the linear regression is equal to the first order apparent rate constant k. Their corresponding values for three levels of TiO_2 (0.1%, 0.3%, and 0.5%) and different initial concentrations of FA (1.2 and 2.4 mmol FA L^{-1}).

Photocatalytic degradation of organic compounds typically follows first-order-kinetics. However, the reaction rate varies with the complexity of the degradation, the amount of substrate adsorbed on the catalyst surface and the absorption spectra of the substrate. Studies with nanomaterials/TiO_2 (nanotubes, nanocylinders, nanoplates, nanospheres, and nanoparticles) with adjusted structural and textural properties were evaluated in the photocatalytic degradation process of FA under UV conditions. FA adsorption isotherms follow the Langmuir model and the kinetics of FA photodegradation shows the Langmuir–Hinshelwood model, regardless of TiO_2 morphologies [67]. When substrates with high UV absorption coefficients are used in excess, they cover the surface of the catalyst and prevent radiation penetration [68]. For the degradation of the FA in the initial concentrations of 1.2 and 2.4 mmol L^{-1}, the degradation reactions occurred in two stages, one fast (1 stage) between 0 and 120 min and the other slow (2 stage) between 120 and 240 min. Since it is a real effluent, the kinetics in two stages is not found by other authors who work with synthetic effluents that only verified the kinetics of the reaction in a single stage [69].

The pseudo-first rate (k) order constants (Table 3) were determined after linearization of the isotherms. The linearization curves for different levels of TiO_2, were calculated from Figs. 10 and 11. For the 0.1% TiO_2 level, the values obtained for k are equal to 0.0020 min^{-1} (1 stage), 0.0085 min^{-1} (2 stage), 0.0043 min^{-1} (1 stage), and 0.0098 min^{-1} (1 stage) for initial concentrations of 1.2 and 2.4 mmol FA L^{-1}, respectively.

Also according to Table 3, for the 0.3% level of TiO_2 the values obtained for k are equal to 0.0031 min^{-1} (1 stage), 0.0091 min^{-1} (2 stage), 0.0037 min^{-1} (1 stage), and 0.0127 min^{-1} (2 stage) for initial concentrations of 1.2, and 2.4 mmol FA L^{-1}, respectively. For the 0.5% TiO_2 level, the values obtained for k are equal to 0.0029 min^{-1} (1 stage), 0.0115 min^{-1} (2 stage), 0.0041 min^{-1} (1 stage), and 0.0137 min^{-1} (2 stage) for initial concentrations of 1.2 and 2.4 mmol FA L^{-1}, respectively. Kinetic rate constants are significant parameters of a degradation process that must be precisely determined, since only a slight change in them will result in a considerable change in the final characteristics of a degradation project [70]. From Table 3, it is possible to observe that the kinetic constants of the degradation reactions increased with the catalyst loads (0.1%, 0.3%, and 0.5%) and the C_0 and C_f concentrations of the FA, which indicates that the initial concentration of the effluent has a significant effect on the rates of degradation, since the constant rate of degradation is higher when the initial concentration of the effluent is higher.

Linear regressions for the different concentrations of TiO_2 were calculated, for TiO_2 of 0.1%, R^2 = 0.9984 (1 stage), R^2 = 0.9604 (2 stage), R^2 = 0.9858 (1 stage), and R^2 = 0.9852 (2 stage), for initial concentrations of 1.2, and 2.4 mmol FA L^{-1}, respectively. While for 0.3% TiO_2, R^2 = 0.9671 (1 stage), R^2 = 0.9962 (2 stage), R^2 = 0.9764 (1 stage), and R^2 = 0.9365 (2 stage), for initial concentrations of 1.2, and 2.4 mmol FA L^{-1}, respectively. For the 0.5% TiO_2 concentration, R^2 = 0.9688 (1 stage), R^2 = 0.9210 (2 stage), R^2 = 0.9723 (1 stage), and R^2 = 0.9953 (2 stage), for initial concentrations of 1.2 and 2.4 mmol FA L^{-1}, respectively. This clearly indicates that the FA degradation reaction present in the effluent obeys first-order-kinetics, occurring in two stages.

3.6. Calculation of the efficiency of removal of organic matter

The efficiency of removing organic matter at reaction time t (min) was calculated using Eq. (11):

$$R = \frac{COD_i - COD_f}{COD_i} \times 100 \quad (11)$$

where R is the % reduced by the process; COD_i is the initial concentration of organic matter (mg O_2 L^{-1}); COD_f is the final concentration of organic matter (mg O_2 L^{-1}).

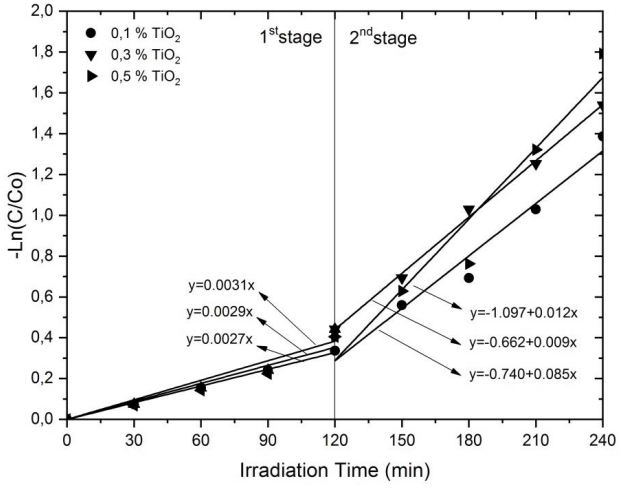

Fig. 10. Linear transformation in $(C/C_0) = f(t)$ of the disappearance of FA (1.1 mmol L^{-1}).

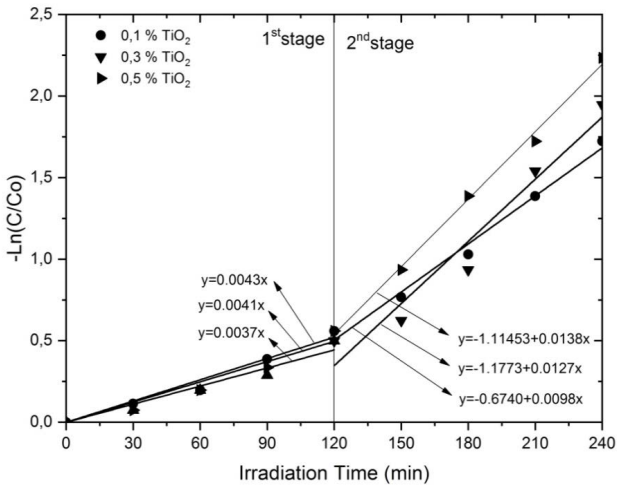

Fig. 11. Linear transformation in $(C/C_0) = f(t)$ of the disappearance of FA (2.2 mmol L^{-1}).

Table 3
Kinetic parameters in the degradation of FA after photocatalytic reactions

TiO_2 (%m/v)	C_0 (mmol L^{-1})	C_f (mmol L^{-1})	η (%)	Stage	k (min^{-1})	$t_{½}$ (min)	R^2
0.1	1.25	0.85	32.00	1	0.0020	346.57	0.9984
	0.85	0.31	63.52	2	0.0085	81.54	0.9604
	2.38	1.36	42.85	1	0.0043	159.71	0.9858
	1.36	0.42	69.11	2	0.0098	70.58	0.9852
0.3	1.25	0.76	39.20	1	0.0031	223.59	0.9671
	0.76	0.25	67.10	2	0.0091	76.17	0.9962
	2.38	1.44	39.49	1	0.0037	187.33	0.9764
	1.44	0.34	76.38	2	0.0127	54.57	0.9365
0.5	1.25	0.85	33.07	1	0.0029	235.76	0.9688
	0.85	0.21	75.29	2	0.0115	60.27	0.9210
	2.38	1.36	42.85	1	0.0041	169.06	0.9723
	1.36	0.25	81.48	2	0.0137	50.26	0.9953

Table 4
COD reduction percentage

TiO_2 load (%)	Initial FA concentration (mmol L^{-1})	Initial COD (mg O_2 L^{-1})	Final COD (mg O_2 L^{-1})	% Reduction
0.1	1.2	164.44	50.85	69.08
	2.4	204.59	56.39	72.44
0.3	1.2	164.44	39.60	75.92
	2.4	204.59	46.61	77.22
0.5	1.2	164.44	35.32	78.52
	2.4	204.59	42.06	79.44

The COD reduction percentage is shown in Table 4, proving that the best parameters relating to the initial concentration of the effluent and the load of the photocatalyst, was with the initial concentration of 2.4 mmol FA L^{-1} and load of the photocatalyst of 0.5%, showing a COD reduction of 79.44%.

Therefore, it was possible to observe that as FA was degraded, the COD reduction rate increased, this means that the organic matter present in the effluent was decomposed into CO_2 and H_2O. Thus, we have that the organic matter has been mineralized, causing a reduction in COD.

4. Conclusions

In the analysis of TiO_2 by granulometry, textural, and SEM it was found an average diameter of particles and pores, as well as a mesoporous structure that act favoring the photocatalytic process. Through thermal analysis it was evident that the endothermic peaks from molecular water such as adsorbed on TiO_2. By XRD and FTIR, it was observed that TiO_2 presented a crystalline structure and characteristic bands of the semiconductor. Significant differences were observed in the degradation of the effluent using the photolysis and photocatalysis process (TiO_2/UV). In the photocatalytic process, the degradation of FA was efficient for the concentration of 2.4 mmol FA L^{-1} of the effluent and 0.5% of TiO_2, with an FA removal of 88.26% and a reduction in the COD of 79.44%. In addition, the calculated kinetics of the process indicated that the degradation of the FA can be divided into two stages, a faster one up to 120 min and a slower one between 120 and 240 min. Therefore, TiO_2/UV photocatalysis can be used as a promising process for FA photodegradation.

References

[1] C. Kahrs, M. Metze, C. Fricke, J. Schwellenbach, Thermodynamic analysis of polymer solutions for the production of polymeric membranes, J. Mol. Liq., 291 (2019) 1–12.
[2] V. Dhineshkumar, D. Ramasamy, Review on membrane technology applications in food and dairy processing, J. Appl. Biotechnol. Bioeng., 3 (2017) 399–407.
[3] T. Marino, F. Galiano, S. Simone, A. Figoli, DMSO EVOL™ as novel non-toxic solvent for polyethersulfone membrane preparation, Environ. Sci. Pollut. Res., 26 (2019) 14774–14785.
[4] K.M. Medeiros, E.M. Araujo, H.L. Lira, D.F. Lima, C.A.P Lima, G.G.C. Lima, Analysis of pore size of hybrid membranes for separation of microemulsions, Desal. Water Treat., 110 (2018) 65–75.
[5] M. Mulder, Basic Principles of Membrane Technology, 2nd ed., Kluwer Academic Publishers, Springer, Netherlands, 1996.
[6] R.W. Baker, Membrane Technology and Applications, 2nd ed., John Wiley & Sons Ltd., Menlo Park, 2004.
[7] M. Razali, J.F. Kim, M. Attfield, P.M. Budd, E. Drioli, Y.M. Leeb, G. Szekely. Sustainable wastewater treatment and recycling in membrane manufacturing, Green Chem., 17 (2015) 5196–5205.

[8] C.H. Loh, B. Wu, L. Ge, C. Pan, R. Wang, High-strength *N*-methyl-2-pyrrolidone-containing process wastewater treatment using sequencing batch reactor and membrane bioreactor: a feasibility study, Chemosphere, 194 (2018) 534–542.
[9] P. Dou, J. Song, S. Zhao, S. Xu, X. Li, T. He, Novel low cost hybrid extraction-distillation-reverse osmosis processfor complete removal of *N*,*N*-dimethylformamide from industrial wastewater, Process Saf. Environ. Prot., 130 (2019) 317–325.
[10] D. Bahnemann, Photocatalytic water treatment: solar energy applications, Sol. Energy, 77 (2004) 445–459.
[11] U.I. Gaya, A.H. Abdullah, M.Z. Hussein, Z. Zainal, Photocatalytic removal of 2,4,6-trichlorophenol from water exploiting commercial ZnO powder, Desalination, 263 (2010) 176–182.
[12] B. Kim, D. Kim, D. Cho, S. Cho, Bactericidal effect of TiO_2 photocatalyst on selected food-borne pathogenic bacteria, Chemosphere, 52 (2003) 277–281.
[13] L. Soares, A. Alves, Photocatalytic properties of TiO_2 and TiO_2/WO_3 films applied as semiconductors in heterogeneous photocatalysis, Mater. Lett., 211 (2018) 339–342.
[14] D. Friedmann, A. Hakki, H. Kim, W. Choic, D. Bahnemann, Heterogeneous photocatalytic organic synthesis: state-of-the-art and future perspectives, Green Chem., 18 (2016) 5391–5411.
[15] L. Chen, J. Tang, L.N. Song, P. Chen, J. He, C. Au, S. Yin, Heterogeneous photocatalysis for selective oxidation of alcohols and hydrocarbons, Appl. Catal., B, 242 (2019) 379–388.
[16] O. Carp, C.L. Huisman, A. Reller, Photoinduced reactivity of titanium dioxide, Prog. Solid State Chem., 32 (2004) 33–177.
[17] J. Schneider, M. Matsuoka, M. Takeuchi, J. Zhang, Y. Horiuchi, M. Anpo, D.W. Bahnemann, Understanding TiO_2 photocatalysis: mechanisms and materials, Chem. Rev., 114 (2014) 9919–9986.
[18] M. Yasmina, K. Mourad, S.H. Mohammed, C. Khaoula, Treatment heterogeneous photocatalysis; factors influencing the photocatalytic degradation by TiO_2, Energy Procedia, 50 (2014) 559–566.
[19] R.S.B. Ferreira, C.H.Ó. Pereira, E.A. Santos Filho, A.M.D. Leite, E.M. Araújo, H.L. Lira, Coagulation bath in the production of membranes of nanocomposites polyamide 6/Clay, Mater. Res., 20 (2017) 117–125.
[20] M.A.Y. Cervantes, J.L.S. Garcıa, M.I.L. Bastarrachea, S.D. Aranda, F.A.R. Trevino, M.A. Vega, Sulfonated polyphenylsulfone asymmetric membranes: effect of coagulation bath (acetic acid-$NaHCO_3$/isopropanol) on morphology and antifouling properties, J. Appl. Polym. Sci., 134 (2016) 1–10.
[21] A.B. Sadi, R.K. Bilali, S.A. Abubshait, H. Kochkar, Low temperature design of titanium dioxide anatase materials decorated with cyanuric acid for formic acid photodegradation, J. Saudi Chem. Soc., 24 (2020) 351–363.
[22] R.B. Baird, A.D. Eaton, E.W. Rice, Standard Methods for the Examination of Water and Wastewater, 23rd ed., American Public Health Association, Washington, DC, 2017.
[23] P. Ngaotrakanwiwat, P. Heawphet, P. Rangsunvigit, Enhancement of photoelectrochemical cathodic protection of copper in marine condition by Cu-doped TiO_2, Catalysts, 10 (2020) 146–155.
[24] X. Yang, Y. Wang, L. Zhang, H. Fu, P. He, D. Han, T. Lawson, X. An, The use of tunable optical absorption plasmonic Au and Ag decorated TiO_2 structures as efficient visible light photocatalysts, Catalysts, 10 (2020) 139–153.
[25] S. Joseph, B. Mathew, Microwave assisted biosynthesis of silver nanoparticles using the rhizome extract of alpinia galanga and evaluation of their catalytic and antimicrobial activities, J. Nanopart., 2014 (2014) 1–9.
[26] K. Dai, H. Chen, T. Peng, D. Ke, H. Yi, Photocatalytic degradation of methyl orange in aqueous suspension of mesoporous titania nanoparticles, Chemosphere, 69 (2007) 1361–1367.
[27] J. Vakros, The influence of preparation method on the physicochemical characteristics and catalytic activity of Co/TiO_2 catalysts, Catalysts, 10 (2020) 88–103.
[28] X. Qin, L. Jing, G. Tiana, Y. Qu, Y. Feng, Enhanced photocatalytic activity for degrading rhodamine B solution of commercial Degussa P25 TiO_2 and its mechanisms, J. Hazard. Mater., 172 (2009) 1168–1174.
[29] V.G. Bessergenev, M.C. Mateus, A.M.B. Rego, M. Hantuschc, E. Burkel, An improvement of photocatalytic activity of TiO_2 degussa P25 powder, Appl. Catal., A, 500 (2015) 42–50.
[30] M. Šihor, M. Reli, M. Vaštyl, K. Hrádková, L. Matejová, K. Kocí, Photocatalytic oxidation of methyl tert-butyl ether in presence of various phase compositions of TiO_2, Catalysts, 10 (2020) 35–47.
[31] S.M. El-Sheikh, T.M. Khedr, A. Hakki, A.A. Ismail, W.A. Badawy, D.W. Bahnemann, Visible light activated carbon and nitrogen Co-doped mesoporous TiO_2 as efficient photocatalyst for degradation of ibuprofen, Sep. Purif. Technol., 173 (2017) 258–268.
[32] S.M. Amorim, J. Suave, L. Andrade, A.M. Mendes, H.J. José, R.F.P.M. Moreira, Towards an efficient and durable self-cleaning acrylic paint containing mesoporous TiO_2 microspheres, Prog. Org. Coat., 118 (2018) 48–56.
[33] A.D. Vishwanath, J.S. Shankar, N.M. Eknath, A.A. Eknath, K.N. Haribhau, Preparation, characterization and photocatalytic activities of TiO_2 towards methyl red degradation, Orient. J. Chem., 33 (2017) 104–112.
[34] I.H. Choi, Y.C. Cho, G. Moon, H.N. Kang, Y.B. Oh, J.Y. Lee, J. Kang, Recent developments in the recycling of spent selective catalytic reduction catalyst in South Korea, Catalysts, 10 (2019) 182–203.
[35] D. Chen, L. Cao, F. Huang, P. Imperia, Y.B. Cheng, R.A. Caruso. Synthesis of monodisperse mesoporous titania beads with controllable diameter, high surface areas, and variable pore diameters (14–23 nm), J. Am. Chem. Soc., 132 (2010) 4438–4444.
[36] C. Marinescu, A. Sofronia, C. Rusti, R. Piticescu, V. Badilita, E. Vasile, R. Baies, S. Tanasescu, DSC investigation of nanocrystalline TiO_2 powder, J. Therm. Anal. Calorim., 103 (2011) 49–57.
[37] S.D. Delekar, H.M. Yadav, S.N. Achary, S.S. Meena, S.H. Pawar, Structural refinement and photocatalytic activity of Fe-doped anatase TiO_2 nanoparticles, Appl. Surf. Sci., 263 (2012) 536–545.
[38] J.C. Yu, J. Yu, W. Ho, Z. Jiang, L. Zhang, Effects of F^- Doping on the photocatalytic activity and microstructures of nanocrystalline TiO_2 powders, Chem. Mater., 14 (2002) 3808–3816.
[39] V.G. Gandhi, M.K. Mishra, M.S. Rao, A. Kumar, P.A. Joshi, D.O. Shah, Comparative study on nano-crystalline titanium dioxide catalyzed photocatalytic degradation of aromatic carboxylic acids in aqueous medium, J. Ind. Eng. Chem., 17 (2011) 331–339.
[40] S.J. Darzi, A.R. Mahjoub, A. Nilchi, Synthesis of spongelike mesoporous anatase and its photocatalytic properties, J. Chem. Chem. Eng., 29 (2010) 37–42.
[41] J. Liu, Q. Zhang, J. Yang, H. Ma, M.O. Tade, S. Wang, J. Liu, Facile synthesis of carbon-doped mesoporous anatase TiO_2 for the enhanced visible-light driven photocatalysis, Chem. Commun., 50 (2014) 13971–13974.
[42] A.G.S. Galdino, E.M. Oliveira, F.B.F. Monteiro, C.A.C. Zavaglia, Analysis of *in vitro* tests of the 50% HA-50% TiO_2 composite manufactured using the polymeric sponge method, Ceramics, 60 (2014) 586–593.
[43] Z. Ma, X. Ma, X. Wang, N. Liu, X. Liu, B. Hou, Study on the photocathodic protection of Q235 steel by $CdIn_2S_4$ sensitized TiO_2 composite in splash zone, Catalysts, 9 (2019) 1067–1080.
[44] A. Matioli, J. Miagava, D. Gouvêa, Modification of the stability of nanometric TiO_2 polymorphs by excess SnO_2 surface, Ceramics, 58 (2012) 53–57.
[45] H. Zangeneh, A.A.L. Zinatizadeh, M. Habibi, M. Akia, M.H. Isa, Photocatalytic oxidation of organic dyes and pollutants in wastewater using different modified titanium dioxides: a comparative review, J. Ind. Eng. Chem., 26 (2015) 1–36.
[46] R. Qian, H. Zong, J. Schneider, G. Zhou, T. Zhao, Y. Li, J. Yang, D.W. Bahnemann, J.H. Pan, Charge carrier trapping, recombination and transfer during TiO2 photocatalysis: an overview, Catal. Today, 335 (2019) 78–90.
[47] S. Sohrabnezhad, Study of catalytic reduction and photodegradation of methylene blue by heterogeneous catalyst, Spectrochim. Acta, Part A, 81 (2011) 228–235.
[48] J. Dostanic, B. Grbic, N. Radic, S. Stojadinovic, R. Vasilic, Z. Vukovic, Preparation and photocatalyic properties of TiO_2-P25

film prepared by spray pyrolysis method, Appl. Surf. Sci., 274 (2013) 321–327.
[49] B. Choudhury, A. Choudhury, Luminescence characteristics of cobalt doped TiO_2 nanoparticles, J. Lumin., 132 (2012) 178–184.
[50] L.G. Devi, B.N. Murhty, S.G. Kumar, Photo catalytic degradation of imidachloprid under solar light using metal ion doped TiO_2 nano particles: influence of oxidation state and electronic configuration of dopants, Catal. Lett., 130 (2009) 496–503.
[51] V.G. Gandhi, M.K. Mishra, P.A. Joshi, A study on deactivation and regeneration of titanium dioxide during photocatalytic degradation of phthalic acid, J. Ind. Eng. Chem., 18 (2012) 1902–1907.
[52] T. Venkov, K. Hadjiivanov, FTIR study of CO interaction with Cu/TiO_2, Catal. Commun., 4 (2003) 209–213.
[53] P.C.S. Bezerra, R.P. Cavalcante, A. Garcia, H. Wender, M.A.U. Martines, G.A. Casagrande, J. Giménez, P. Marco, S.C. Oliveira, A. Machulek Jr., Synthesis, characterization, and photocatalytic activity of pure and N-, B-, or Ag-doped TiO_2, J. Braz. Chem. Soc., 28 (2017) 1788–1802.
[54] G. Szekely, M.F. Jimenez-Solomon, P. Marchetti, J.F. Kim, A.G. Livingston, Sustainability assessment of organic solvent nanofiltration: from fabrication to application, Green Chem., 16, (2014) 4440–4473.
[55] F. Riboni, M.V. Dozzi, M.C. Paganini, E. Giamello, E. Selli, Photocatalytic activity of TiO_2-WO_3 mixed oxides in formic acid oxidation, Catal. Today, 287 (2017) 176–181.
[56] P.L.K. Ardila, B.F. Silva, M. Spadoto, B.C.M. Rispoli, E.B. Azevedo, Which route to take for diclofenac removal from water: hydroxylation or direct photolysis?, J. Photochem. Photobiol., A, 382 (2019) 1–7.
[57] V. Augugliaro, M. Bellardita, V. Loddo, G. Palmisano, L. Palmisano, S. Yurdakal, Overview on oxidation mechanisms of organic compounds by TiO_2 in heterogeneous photocatalysis, J. Photochem. Photobiol., C, 13 (2012) 224–245.
[58] T. Ma, S. Garg, C.J. Miller, T.D. Waite, Contaminant degradation by irradiated semiconducting silver chloride particles: kinetics and modelling, J. Colloid Interface Sci., 446 (2015) 366–372.
[59] N. Negishi, M. Sugasawa, Y. Miyazaki, Y. Hirami, S. Koura, Effect of dissolved silica on photocatalytic water purification with a TiO_2 ceramic catalyst, Water Res., 150 (2019) 40–46.
[60] M. Hamandi, G. Berhault, C. Guillard, H. Kochkar, Influence of reduced graphene oxide on the synergism between rutile and anatase TiO_2 particles in photocatalytic degradation of formic acid, Mol. Catal., 432 (2017) 125–130.
[61] W. El-Alami, D.G. Sousa, C.F. Rodríguez, O.G. Díaz, J.M.D. Rodríguez, M.E. Azzouzi, J. Araña, Efect of Ti-F surface interaction on the photocatalytic degradation of phenol, aniline and formic acid, J. Photochem. Photobiol., A, 348 (2017) 139–149.
[62] K.L. Miller, C.W. Lee, J.L. Falconer, J.W. Medlin, Effect of water on formic acid photocatalytic decomposition on TiO_2 and Pt/TiO_2, J. Catal., 275 (2010) 294–299.
[63] S. Papoutsakis, S.M. Cuevas, N. Gondrexon, S. Baup, S. Malato, C. Pulgarin, Coupling between high-frequency ultrasound and solar photo-Fenton at pilot scale for the treatment of organic contaminants: an initial approach, Ultrason. Sonochem., 22 (2015) 527–534.
[64] P. Anca, M.C. Anca, C. Nicula, L.M. Cozmuta, A. Jastrzębska, A. Olszyna, L. Baia, UV light-assisted degradation of methyl orange, methylene blue, phenol, salicylic acid, and rhodamine B: photolysis versus photocatalyis, Water Air Soil Pollut., 228 (2017) 28–41.
[65] T. Soltani, M.H. Entezari, Photolysis and photocatalysis of methylene blue by ferrite bismuth nanoparticlesunder sunlight irradiation, J. Mol. Catal. A: Chem., 377 (2013) 197–203.
[66] M. Sanchez, M.J. Rivero, I. Ortiz, Kinetics of dodecylbenzenesulphonate mineralisation by TiO_2 photocatalysis, Appl. Catal., B, 101 (2011) 515–521.
[67] A.Turki, C. Guillard, F. Dappozze, G. Berhault, Z. Ksibi, H. Kochkar, Design of TiO_2 nanomaterials for the photo-degradation of formic acid - adsorption isotherms and kinetics study, J. Photochem. Photobiol., A, 279 (2014) 8–16.
[68] W.S. Lopes, M.G.C. Azevedo, V.D. Leite, J.T. Sousa, J.S. Buriti, Degradation of 17α-ethinylestradiol in water by heterogeneous photocatalysis, Environ. Water Interdiscip. J. Appl. Sci., 10 (2015) 728–736.
[69] S. Wang, F. Shiraishi, K. Nakano, A synergistic effect of photocatalysis and ozonation on decomposition of formic acid in an aqueous solution, Chem. Eng. J., 87 (2002) 261–271.
[70] J.F. Montoya, J.A. Velásquez, P. Salvador, The direct-indirect kinetic model in photocatalysis: a reanalysis of phenol and formic acid degradation rate dependence on photon flow and concentration in TiO_2 aqueous dispersions, Appl. Catal., B, 88 (2009) 50–58.